

Photoproduction of P -wave doubly charmed baryon at future e^+e^- collider

Xi-Jie Zhan,^{a,b,1} Xing-Gang Wu,^{a,b} Xu-Chang Zheng^{a,b}

^a*Department of Physics, Chongqing University,
Chongqing 401331, People's Republic of China*

^b*Chongqing Key Laboratory for Strongly Coupled Physics, Chongqing University,
Chongqing 401331, People's Republic of China*

E-mail: zhanxj@cqu.edu.cn, wuxg@cqu.edu.cn, zhengxc@cqu.edu.cn

ABSTRACT: The photoproduction of P -wave doubly charmed baryon (Ξ_{cc}) is investigated in the context of future high-energy and high-luminosity e^+e^- colliders. The direct photoproduction via the sub-process $\gamma + \gamma \rightarrow \Xi_{cc} + \bar{c} + \bar{c}$ and the resolved channel $\gamma + g \rightarrow \Xi_{cc} + \bar{c} + \bar{c}$ are considered. Within the framework of non-relativistic QCD, the calculation encompasses four P -wave (cc) -diquark configurations: $(cc)_{\mathbf{\bar{3}}}[^1P_1]$, $(cc)_{\mathbf{6}}[^3P_0]$, $(cc)_{\mathbf{6}}[^3P_1]$ and $(cc)_{\mathbf{6}}[^3P_2]$. The two S -wave states, $(cc)_{\mathbf{\bar{3}}}[^3S_1]$ and $(cc)_{\mathbf{6}}[^1S_0]$, are also included for comparison. The cross sections, as well as the differential distributions involving transverse momentum, rapidity, and angular variables, have been computed. Numerical results reveal that the resolved photoproduction process plays a significant role and can provide dominant contributions. The photoproduction rate of the P -wave Ξ_{cc} is approximately one order of magnitude lower than that of the S -wave.

¹Corresponding author.

Contents

1	Introduction	1
2	Formulation and calculation	2
3	Numerical results and discussions	6
4	Summary	9

1 Introduction

A doubly heavy baryon is a system composed of two heavy quarks and one light quark. It possesses a simple structure akin to that of a heavy quarkonium, which enables rigorous theoretical analysis. As a result, investigating its production properties is believed to aid in understanding and validating the theory of Quantum Chromodynamics (QCD). In 2002 and 2005, the SELEX Collaboration reported a possible discovery of the Ξ_{cc}^+ baryon [1, 2]. More recently, in 2017, the LHCb Collaboration confirmed the existence of another type of doubly heavy baryon, Ξ_{cc}^{++} , through the decay channel $\Xi_{cc}^{++} \rightarrow \Lambda_c^+ K^- \pi^+ \pi^+$ ($\Lambda_c^+ \rightarrow p K^- \pi^+$). The measured properties of mass and lifetime for this Ξ_{cc}^{++} baryon were found to be in excellent agreement with theoretical calculations. Subsequently, the LHCb Collaboration further confirmed its existence in the decay $\Xi_{cc}^{++} \rightarrow \pi^+ \Xi_c^+$ [3, 4]. The genuine discovery of doubly heavy baryons is poised to trigger a new wave of theoretical research.

Due to the inherent nonrelativistic characteristics coupled with the confinements attributed to strong interactions, the production of doubly heavy baryons encompasses intricate nonperturbative effects that elude computation through conventional perturbative QCD methods. The study conducted by Ma et al. [5] undertook the task of describing this production process through the utilization of the nonrelativistic QCD (NRQCD) factorization framework [6]. This ingenious framework dissects the procedure into two sequential stages: firstly, the perturbative formation of a heavy-quark pair within a distinct quantum state, often referred to as a diquark, followed by its subsequent nonperturbative transformation into a baryon. By employing an expansion rooted in the heavy quark's diminished velocity (v_Q) within the rest frame of the baryon, the study was able to pinpoint two foremost states of (cc)-diquarks at the leading order: $\bar{\mathbf{3}}[{}^3S_1]$ and $\mathbf{6}[{}^1S_0]$. These diquark states respectively correspond to the 3S_1 and 1S_0 S-wave configurations, while existing in the $\bar{\mathbf{3}}$ and $\mathbf{6}$ color states. Accompanying these states are the associated long-distance matrix elements (LDMEs), denoted as $h_{\bar{\mathbf{3}}}$ and $h_{\mathbf{6}}$, which encapsulate the nonperturbative likelihood of their transition into the baryonic state.

Numerous comprehensive theoretical investigations have delved into the realm of producing doubly heavy baryons [7–34]. These investigations have encompassed a range of

production mechanisms, including direct processes occurring in pp , ep , $\gamma\gamma$, and e^+e^- collisions, as well as indirect channels involving the decays of Higgs bosons, W and Z bosons, and top quarks. For the purpose of simulating hadroproduction in pp collisions, a dedicated generator known as GENXICC [35–37] has been meticulously developed.

Next-generation e^+e^- colliders have been put forth in recent times, among them being the FCC-ee [38], the CEPC [39, 40], and the ILC [41, 42]. These cutting-edge colliders are designed to operate at high collision energies and are projected to achieve unparalleled luminosities. As a result of their capabilities, these advanced e^+e^- colliders hold immense potential to serve as exceptional platforms for a wide array of research topics. The e^+e^- collider provides two main pathways for the direct production of the doubly heavy baryon Ξ_{cc} : production through e^+e^- annihilation and via the photoproduction mechanism. In this work, Ξ_{cc} denotes the baryon Ξ_{ccq} , where q corresponds to an up (u), down (d), or strange (s) quark. Regarding photoproduction, the Ξ_{cc} baryon can be generated through direct photon-photon fusion, such as $\gamma + \gamma \rightarrow \Xi_{cc} + \bar{c} + \bar{c}$. Beyond direct photoproduction, another category of processes, known as resolved photoproduction [43], exists. In these cases, the photon undergoes a process of resolution, leading to its parton's involvement in the subsequent hard processes. The resolved photoproduction channels share a comparable order of perturbative expansion with the direct approach, underscoring the need for their incorporation in calculations. Earlier investigations [43–48] have indicated that the single resolved channel ($\gamma + g$) tend to exert a dominant influence on the photoproduction of heavy quarkonium and doubly heavy baryon at e^+e^- colliders. The contributions stemming from double resolved photoproduction channels are generally negligible and can be safely ignored.

In this work, we offer an analysis of the photoproduction of P -wave doubly charmed baryon at future e^+e^- collider. Based on the NRQCD factorization framework, we will consider two types of photoproduction processes: $\gamma + \gamma \rightarrow \Xi_{cc} + \bar{c} + \bar{c}$ and $\gamma + g \rightarrow \Xi_{cc} + \bar{c} + \bar{c}$. For (cc) -diquark, the quantum number is $(cc)_{\mathbf{3}}[{}^3S_1]$, $(cc)_{\mathbf{6}}[{}^1S_0]$, $(cc)_{\mathbf{3}}[{}^1P_1]$ or $(cc)_{\mathbf{6}}[{}^3P_J]$ with $J = 0, 1, 2$. Section 2 provides the formulation of the calculation, while Section 3 presents the numerical results and subsequent discussions. Section 4 gives a brief summary.

2 Formulation and calculation

At future e^+e^- colliders, the initial photons possess the capacity to attain both high energy and luminosity via laser back-scattering(LBS). This phenomenon is expounded upon in the spectrum detailed by Ginzburg et al. [49],

$$f_{\gamma/e}(x) = \frac{1}{N} \left[1 - x + \frac{1}{1-x} - 4r(1-r) \right], \quad (2.1)$$

where $x = E_\gamma/E_e$, $r = x/(x_m(1-x))$, and the normalization factor is given by:

$$N = \left(1 - \frac{4}{x_m} - \frac{8}{x_m^2} \right) \log(1+x_m) + \frac{1}{2} + \frac{8}{x_m} - \frac{1}{2(1+x_m)^2}. \quad (2.2)$$

Here, $x_m = 4E_e E_l \cos^2 \frac{\theta}{2}$, with E_e and E_l representing the energies of the incident electron and laser beams, respectively, and θ denoting the angle between them. The range of energy

for the laser back-scattering (LBS) photon is constrained by:

$$0 \leq x \leq \frac{x_m}{1 + x_m}, \quad (2.3)$$

with the optimal value of x_m being 4.83 [50].

Within the framework of non-relativistic QCD (NRQCD), the photoproduction cross-section of Ξ_{cc} at the e^+e^- collider can be represented as follows:

$$\begin{aligned} & d\sigma(e^+e^- \rightarrow e^+e^-\Xi_c + \bar{c} + \bar{c}) \\ &= \int dx_1 f_{\gamma/e}(x_1) \int dx_2 f_{\gamma/e}(x_2) \\ &\times \sum_{i,j} \int dx_i f_{i/\gamma}(x_i) \int dx_j f_{j/\gamma}(x_j) \\ &\times \sum_n d\hat{\sigma}(ij \rightarrow (cc)[n] + \bar{c} + \bar{c}) \langle \mathcal{O}^{\Xi_{cc}}[n] \rangle. \end{aligned} \quad (2.4)$$

Here, $f_{\gamma/e}(x)$ represents the energy spectrum of the photon. $f_{i/\gamma}$ ($i = \gamma, g, u, d, s$) corresponds to the Glück-Reya-Schienbein (GRS) distribution function of parton i within the photon [51]. $f_{\gamma/\gamma}(x) = \delta(1-x)$ is utilized for the direct photoproduction process. $d\hat{\sigma}(ij \rightarrow (cc)[n] + \bar{c} + \bar{c})$ denotes the differential partonic cross-section, which is evaluated perturbatively. For the baryons Ξ_{cc} , $(cc)[n] = (cc)_{\mathbf{\bar{3}}}[^3S_1]$, $(cc)_{\mathbf{6}}[^1S_0]$, $(cc)_{\mathbf{\bar{3}}}[^1P_1]$ or $(cc)_{\mathbf{6}}[^3P_J]$. $\langle \mathcal{O}^{\Xi_{cc}}[n] \rangle = h_{\mathbf{\bar{3}}(\mathbf{6})}$ denotes the long-distance matrix element (LDME). Typically, people adopt a potential model approach, drawing parallels with the heavy quarkonium scenario, and introduce and correlate a wave function with $h_{\mathbf{\bar{3}}}$ [7, 52–55],

$$h_{\mathbf{\bar{3}}} \simeq |\Psi_{cc}(0)|^2 \text{ or } |\Psi'_{cc}(0)|^2. \quad (2.5)$$

Regarding $h_{\mathbf{6}}$, there exists no specific relation, and for the sake of simplicity, it is assumed to be equal to $h_{\mathbf{\bar{3}}}$. This assumption is rooted in NRQCD's power counting relative to v_c , where both $h_{\mathbf{6}}$ and $h_{\mathbf{\bar{3}}}$ are assigned equivalent orders [5]. In accordance with NRQCD, the bound state Ξ_{cc} can be expanded into a series of Fock states:

$$|\Xi_{cc}\rangle = c_1(v)|(cc)q\rangle + c_2(v)|(cc)qg\rangle + c_3(v)|(cc)qgg\rangle + \dots. \quad (2.6)$$

Because a light quark can easily emit gluons, the constituents in Eq. (2.6) carry equivalent significance, specifically, $c_1 \sim c_2 \sim c_3$. Consider a cc pair in the $\mathbf{\bar{3}}[^3S_1]$ state; one of the heavy quarks can emit a gluon without altering the spin of the heavy quark. Subsequently, this emitted gluon can undergo a splitting process, leading to the formation of a light quark-antiquark pair $q\bar{q}$. This allows the heavy cc pair to interact with the light q and form the composite particle Ξ_{cc} . Similarly, for a cc pair in the $\mathbf{6}[^1S_0]$ state, one of the heavy quarks can emit a gluon while preserving the spin of the heavy quark. This emitted gluon then separates into a light $q\bar{q}$ pair, and the light quarks also have the capability to emit gluons. Consequently, this heavy cc pair can capture a light quark and a gluon to assemble into Ξ_{cc} . This is the reason for $h_{\mathbf{6}}$ and $h_{\mathbf{\bar{3}}}$ holding the same order in v_c . For the sake of simplicity, we assume $h_{\mathbf{6}} = h_{\mathbf{\bar{3}}}$ in the subsequent calculations. It is worth noting that

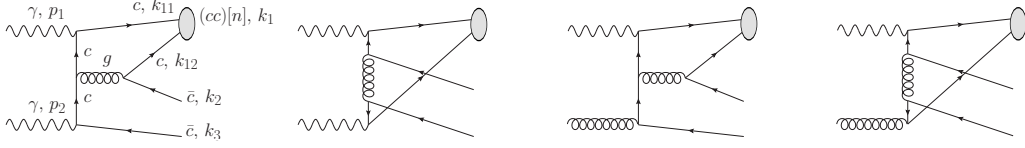


Figure 1. Some Feynman diagrams of the partonic processes for Ξ_{cc} photoproduction. The diagrams are drawn by JaxoDraw [56].

the long-distance matrix elements (LDMEs) function as overarching parameters beyond the perturbative components, indicating that the results can be refined with the acquisition of new LDMEs.

For the partonic processes in leading order of α_s , there are 40 Feynman diagrams for $\gamma + \gamma \rightarrow \Xi_{cc} + \bar{c} + \bar{c}$ and 48 diagrams for $\gamma + g \rightarrow \Xi_{cc} + \bar{c} + \bar{c}$, as exemplified in Fig. 1. In practical calculations, we apply charge conjugation $C = -i\gamma^2\gamma^0$ to reverse the one of the $c \sim \bar{c}$ fermion chains, such as $L_1 = \bar{u}_{s_1}(k_{12})\Gamma_{i+1}S_F(q_i, m_i) \cdots S_F(q_1, m_1)\Gamma_1 v_{s_2}(k_2)$. Here, Γ_i represents the interaction vertex, $S_F(q_i, m_i)$ denotes the fermion propagator, where q_i and m_i are the respective momentum and mass parameters. The subscripts s_1 and s_2 are used for spin indices, while the index i enumerates the fermion propagators ($i = 0, 1, \dots$) along this fermion line. The conversion obeys:

$$\begin{aligned}
v_{s_2}^T(k_2)C &= -\bar{u}_{s_2}(k_2), \\
C^{-1}\bar{u}_{s_1}(k_{12})^T &= v_{s_1}(k_{12}), \\
C^{-1}S_F^T(-q_i, m_i)C &= S_F(q_i, m_i), \\
C^{-1}\Gamma_i^T C &= -\Gamma_i.
\end{aligned} \tag{2.7}$$

L_1 is reversed to:

$$\begin{aligned}
L_1 &= L_1^T = v_{s_2}^T(k_2)\Gamma_1^T F_F^T(q_1, m_1) \cdots S_F^T(q_i, m_i)\Gamma_{i+1}^T \bar{u}_{s_1}^T(k_{12}) \\
&= v_{s_2}^T(k_2)CC^{-1}\Gamma_1^T CC^{-1}S_F^T(q_1, m_1)CC^{-1} \cdots CC^{-1}S_F^T(q_i, m_i)CC^{-1}\Gamma_{i+1}^T CC^{-1}\bar{u}_{s_1}^T(k_{12}) \\
&= (-1)^{(n+1)}\bar{u}_{s_2}(k_2)\Gamma_1 S_F(-q_1, m_1) \cdots S_F(-q_i, m_i)\Gamma_{i+1} v_{s_1}(k_{12}),
\end{aligned} \tag{2.8}$$

here n is the number of vector vertices in the fermion chain. Let us take the first diagram in Fig. 1 as an example, its amplitudes read:

$$\begin{aligned}
M_1 &\sim \frac{1}{(k_{12} + k_2)^2} \bar{u}_{s_{12}}(k_{12})\gamma^\mu v_{s_2}(k_2)\bar{u}_{s_{11}}(k_{11}) \not{\epsilon}(p_1) \\
&\quad \frac{\not{p}_2 - \not{k}_{12} - \not{k}_2 - \not{k}_3 + m_c}{(\not{p}_2 - \not{k}_{12} - \not{k}_2 - \not{k}_3)^2 - m_c^2} \gamma^\mu \frac{\not{p}_2 - \not{k}_3 + m_c}{(\not{p}_2 - \not{k}_3)^2 - m_c^2} \not{\epsilon}(p_2) v_{s_3}(k_3),
\end{aligned} \tag{2.9}$$

Where k_{11} and k_{12} are momenta of the two c quarks. In the diquark state, their relative momentum q is small and we can set $k_{11} = \frac{m_c}{M_{cc}}k_1 + q$ and $k_{12} = \frac{m_c}{M_{cc}}k_1 - q$ with k_1 being the momentum of the diquark. Here the diquark mass $M_{cc} = 2m_c$ is adopted in order to ensure the gauge invariance of the amplitude. After reverse the first fermion line, the amplitude

becomes:

$$M_1 \sim -\frac{1}{(k_{12} + k_2)^2} \bar{u}_{s2}(k_2) \gamma^\mu v_{s12}(k_{12}) \bar{u}_{s11}(k_{11}) \not{\epsilon}(p_1) \frac{\not{p}_2 - \not{k}_{12} - \not{k}_2 - \not{k}_3 + m_c}{(\not{p}_2 - \not{k}_{12} - \not{k}_2 - \not{k}_3)^2 - m_c^2} \gamma^\mu \frac{\not{p}_2 - \not{k}_3 + m_c}{(\not{p}_2 - \not{k}_3)^2 - m_c^2} \not{\epsilon}(p_2) v_{s3}(k_3). \quad (2.10)$$

Now we can replace $v_{s12}(k_{12}) \bar{u}_{s11}(k_{11})$ by the spin projector for $(c\bar{c})[n]$ to get the amplitude of $\gamma + \gamma \rightarrow (cc)[n] + \bar{c} + \bar{c}$. The spin projector takes the form of

$$\Pi_{k_1}(q) = \frac{-\sqrt{M_{cc}}}{4m_c^2} (\not{k}_{12} - m_c) \gamma^5 (\not{k}_{11} + m_c), \quad (2.11)$$

$$\Pi_{k_1}^\beta(q) = \frac{-\sqrt{M_{cc}}}{4m_c^2} (\not{k}_{12} - m_c) \gamma^\beta (\not{k}_{11} + m_c), \quad (2.12)$$

for $n = {}^1S_0$ and 3S_1 respectively. The amplitudes of the P -wave production can be obtained via the derivation of the S -wave expression, i.e.,

$$M_1[{}^1P_1] \sim \varepsilon_\alpha^l(k_1) \frac{d}{dq_\alpha} \left[-\frac{1}{(k_{12} + k_2)^2} \bar{u}_{s2}(k_2) \gamma^\mu \frac{-\sqrt{M_{cc}}}{4m_c^2} (\not{k}_{12} - m_c) \gamma^5 (\not{k}_{11} + m_c) \not{\epsilon}(p_1) \frac{\not{p}_2 - \not{k}_{12} - \not{k}_2 - \not{k}_3 + m_c}{(\not{p}_2 - \not{k}_{12} - \not{k}_2 - \not{k}_3)^2 - m_c^2} \gamma^\mu \frac{\not{p}_2 - \not{k}_3 + m_c}{(\not{p}_2 - \not{k}_3)^2 - m_c^2} \not{\epsilon}(p_2) v_{s3}(k_3) \right]_{q=0}, \quad (2.13)$$

$$M_1[{}^3P_J] \sim \varepsilon_{\alpha\beta}^J(k_1) \frac{d}{dq_\alpha} \left[-\frac{1}{(k_{12} + k_2)^2} \bar{u}_{s2}(k_2) \gamma^\mu \frac{-\sqrt{M_{cc}}}{4m_c^2} (\not{k}_{12} - m_c) \gamma^\beta (\not{k}_{11} + m_c) \not{\epsilon}(p_1) \frac{\not{p}_2 - \not{k}_{12} - \not{k}_2 - \not{k}_3 + m_c}{(\not{p}_2 - \not{k}_{12} - \not{k}_2 - \not{k}_3)^2 - m_c^2} \gamma^\mu \frac{\not{p}_2 - \not{k}_3 + m_c}{(\not{p}_2 - \not{k}_3)^2 - m_c^2} \not{\epsilon}(p_2) v_{s3}(k_3) \right]_{q=0}, \quad (2.14)$$

Here, $\varepsilon_\beta^s(k_1)$ or $\varepsilon_\alpha^l(k_1)$ represents the polarization vector associated with the spin or orbital angular momentum of the diquark in the spin triplet S -state or spin singlet P -state. $\varepsilon_{\alpha\beta}^J(k_1)$ corresponds to the polarization tensor for the spin triplet P -wave states, where J can be 0, 1, or 2. To determine the suitable total angular momentum, we appropriately perform the polarization sum. The summation over polarization vectors is carried out as follows:

$$\sum_{r_z} \varepsilon_\alpha^r \varepsilon_{\alpha'}^{r*} = \Pi_{\alpha\alpha'} \quad (2.15)$$

The summation over polarization tensors is conducted as:

$$\varepsilon_{\alpha\beta}^0 \varepsilon_{\alpha'\beta'}^{0*} = \frac{1}{3} \Pi_{\alpha\beta} \Pi_{\alpha'\beta'} \quad (2.16)$$

$$\sum_{J_z} \varepsilon_{\alpha\beta}^1 \varepsilon_{\alpha'\beta'}^{1*} = \frac{1}{2} (\Pi_{\alpha\alpha'} \Pi_{\beta\beta'} - \Pi_{\alpha\beta'} \Pi_{\alpha'\beta}) \quad (2.17)$$

$$\sum_{J_z} \varepsilon_{\alpha\beta}^2 \varepsilon_{\alpha'\beta'}^{2*} = \frac{1}{2} (\Pi_{\alpha\alpha'} \Pi_{\beta\beta'} + \Pi_{\alpha\beta'} \Pi_{\alpha'\beta}) - \frac{1}{3} \Pi_{\alpha\beta} \Pi_{\alpha'\beta'}, \quad (2.18)$$

with the definition

$$\Pi_{\alpha\beta} = -g_{\alpha\beta} + \frac{k_{1\alpha} k_{1\beta}}{M_{cc}^2}. \quad (2.19)$$

$\sqrt{S}(\text{GeV})$	$\gamma + \gamma \rightarrow \Xi_{cc} + \bar{c} + \bar{c}$	$\gamma + g \rightarrow \Xi_{cc} + \bar{c} + \bar{c}$	total
250	228.61	238.90	467.50
500	101.34	411.50	512.84
1000	40.94	659.81	700.75

Table 1. The integrated cross sections (in unit of fb) from different channels for Ξ_{cc} photoproduction under various collision energies at future e^+e^- collider. The contributions from the S -wave and P -wave have been combined.

For the processes $\gamma + \gamma \rightarrow (cc)[n] + \bar{c} + \bar{c}$, the color factor $\mathcal{C}_{ij,k}$ is universal for all the Feynman diagrams and $\mathcal{C}_{ij,k} = \mathcal{N} \times \sum_{a,m,n} (T^a)_{mi} (T^a)_{nj} \times G_{mnk}$. Here $\mathcal{N} = 1/\sqrt{2}$ is the normalization constant, i, j, m, n are color indices of four heavy quarks and k denotes the color index of the diquark. G_{mnk} corresponds to either the antisymmetric function ε_{mnk} for the color anti-triplet state, or the symmetric function f_{mnk} for the color sextuplet state, and they obey

$$\varepsilon_{mnk} \varepsilon_{m'n'k} = \delta_{mm'} \delta_{nn'} - \delta_{mn'} \delta_{nm'}, \quad (2.20)$$

$$f_{mnk} f_{m'n'k} = \delta_{mm'} \delta_{nn'} + \delta_{mn'} \delta_{nm'}. \quad (2.21)$$

The color factors of diagrams for $\gamma + g \rightarrow (cc)[n] + \bar{c} + \bar{c}$ are not the same; they need to be calculated individually.

3 Numerical results and discussions

In the calculation, we adopt the wave functions at the origin from [57] as $|\Psi(0)|^2 = 0.0218 \text{ GeV}^3$ and $|\Psi'(0)|^2 = 2.48 \times 10^{-3} \text{ GeV}^5$. The quark mass is set as $m_c = M_{\Xi_{cc}}/2 = 1.8 \text{ GeV}$. The fine structure constant is assigned the value $\alpha = 1/137$. Regarding the strong coupling constant, we utilize the one-loop running formulation. The renormalization scale is typically taken as the transverse mass of Ξ_{cc} , specifically $\mu = \sqrt{M_{\Xi_{cc}}^2 + p_t^2}$, where p_t denotes the transverse momentum of the particle.

Table 1 lists cross sections of different photoproduction processes, where three collision energies, $\sqrt{S} = 250, 500, 1000 \text{ GeV}$, are adopted. From the table, it is evident that the contribution from production channel $\gamma + \gamma$ decreases as the collision energy increases, while the contribution from production channel $\gamma + g$ increases with higher energy levels. As a cumulative result, the total production cross-section increases with the growth of collision energy. At $\sqrt{S} = 250 \text{ GeV}$, the contribution from the $\gamma + \gamma$ channel is comparable to that of the $\gamma + g$ channel. However, as the collision energy increases, the scenario changes. The $\gamma + g$ channel begins to dominate the photoproduction process. Specifically, at $\sqrt{S} = 500 \text{ GeV}$, the $\gamma + \gamma$ channel provides 20% of the contribution, while the $\gamma + g$ channel contributes 80%. Table 1 clearly emphasizes the significance of the single resolved photoproduction channel.

Similarly, for the three collision energies, cross sections of various intermediate diquark states are provided in Table 2. These results reveal that the contribution of S -wave diquarks is significantly larger than that of the P -wave diquarks. At $\sqrt{S} = 250 \text{ GeV}$, the ratio between the contributions from the S -wave and P -wave is 18.7:1. At $\sqrt{S} = 500 \text{ GeV}$, the ratio

\sqrt{S} (GeV)	$(cc)_{\mathbf{3}}[{}^3S_1]$	$(cc)_{\mathbf{6}}[{}^1S_0]$	$(cc)_{\mathbf{3}}[{}^1P_1]$	$(cc)_{\mathbf{6}}[{}^3P_0]$	$(cc)_{\mathbf{6}}[{}^3P_1]$	$(cc)_{\mathbf{6}}[{}^3P_2]$
250	407.43	36.32	8.81	1.75	2.44	10.75
500	442.71	41.24	9.42	2.12	3.03	14.32
1000	603.0	57.05	12.66	2.97	4.33	20.72

Table 2. The integrated cross sections (in unit of fb) of different intermediate diquark states for Ξ_{cc} photoproduction under various collision energies at future e^+e^- collider.

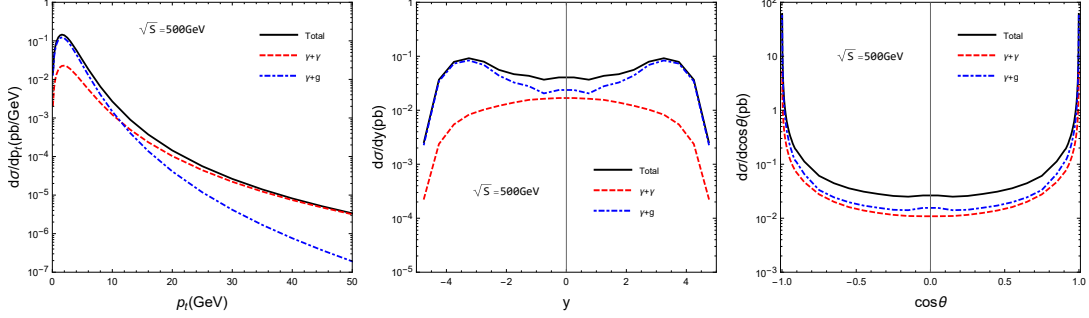


Figure 2. Kinematic distributions for the photoproduction of Ξ_{cc} at future e^+e^- collider ($\sqrt{S} = 500$ GeV). Contributions from different channels are displayed individually.

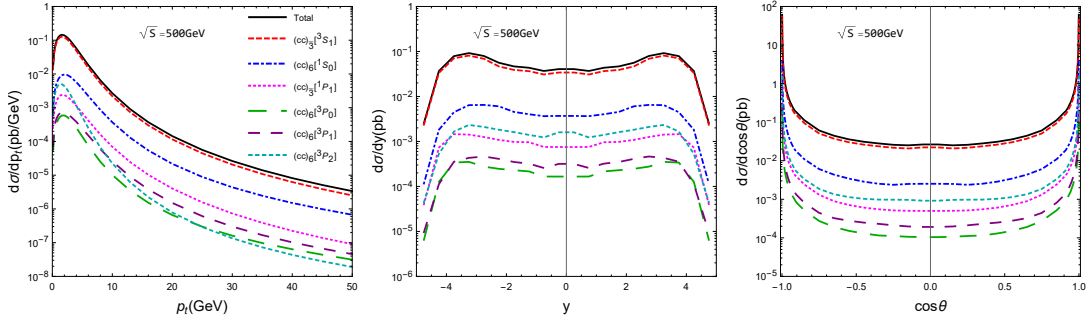


Figure 3. Kinematic distributions for the photoproduction of Ξ_{cc} at future e^+e^- collider ($\sqrt{S} = 500$ GeV). Contributions from different diquark states are displayed individually. The y and $\cos\theta$ curves use same legends as those of p_t .

becomes 16.8:1, meaning that the P -wave contributions constitute 5.6% of the total production. Among the P -wave states, the contribution of the $(cc)_{\mathbf{6}}[{}^3P_2]$ diquark is the largest. Their ratio is as follows: $(cc)_{\mathbf{3}}[{}^1P_1] : (cc)_{\mathbf{6}}[{}^3P_0] : (cc)_{\mathbf{6}}[{}^3P_1] : (cc)_{\mathbf{6}}[{}^3P_2] = 1:0.23:0.32:1.52$ at $\sqrt{S} = 500$ GeV. Assuming an integrated luminosity of $\mathcal{O}(10^4)$ fb^{-1} at future e^+e^- colliders and summing up the contributions from all P -wave excited baryons, approximately 2.9×10^5 P -wave Ξ_{cc} baryons would be generated, given a collision energy of $\sqrt{S} = 500$ GeV. The P -wave doubly charmed baryons are likely to decay to the ground state with almost 100% probability, making them additional sources of ground-state baryons.

To reveal more characteristics of Ξ_{cc} photoproduction at the e^+e^- collider, we have computed the differential distributions at $\sqrt{S} = 500$ GeV, as illustrated in Fig.2 and Fig.3. Fig. 2 depicts the transverse momentum(p_t), the rapidity(y) and $\cos\theta$ distributions, fea-

$m_c(\text{GeV})$	$(cc)_{\bar{3}}[{}^3S_1]$	$(cc)_{\mathbf{6}}[{}^1S_0]$	$(cc)_{\bar{3}}[{}^1P_1]$	$(cc)_{\mathbf{6}}[{}^3P_0]$	$(cc)_{\mathbf{6}}[{}^3P_1]$	$(cc)_{\mathbf{6}}[{}^3P_2]$
1.7	609.62	56.85	14.50	3.28	4.67	22.27
1.8	442.71	41.24	9.42	2.12	3.03	14.32
1.9	328.38	30.53	6.24	1.40	2.0	9.45

Table 3. The total cross sections (in unit of fb) under different m_c at $\sqrt{S} = 500$ GeV.

\mathcal{C}	$(cc)_{\bar{3}}[{}^3S_1]$	$(cc)_{\mathbf{6}}[{}^1S_0]$	$(cc)_{\bar{3}}[{}^1P_1]$	$(cc)_{\mathbf{6}}[{}^3P_0]$	$(cc)_{\mathbf{6}}[{}^3P_1]$	$(cc)_{\mathbf{6}}[{}^3P_2]$
0.5	531.74	50.46	11.44	2.47	3.57	16.40
1.0	442.71	41.24	9.42	2.12	3.03	14.32
2.0	376.96	35.12	8.0	1.84	2.59	12.61

Table 4. The total cross sections (in unit of fb) under various $\mu(= \mathcal{C}\sqrt{M_{\Xi_{cc}}^2 + p_t^2})$ with $\mathcal{C} = 0.5, 1, 2$ at $\sqrt{S} = 500$ GeV.

turing distinct representations of contributions originating from different channels. Here, θ represents the angle between Ξ_{cc} and the e^+e^- beams. The $\gamma + g$ channels exert their dominance in the lower p_t region, gradually passing the torch to the $\gamma + \gamma$ channels as the p_t values increase. In practical experiments, there may not be a sufficient number of events in the high p_t region to attain precise measurements. Consequently, it becomes necessary to consider the single resolved channel $\gamma + g$ when performing photoproduction calculations. In contrast to the curves for the p_t distribution, in the rapidity and angular distributions, the curves for the two production channels do not intersect. Throughout the entire rapidity distribution range, the contributions of $\gamma + g$ consistently surpass those of $\gamma + \gamma$. The same pattern is also evident in the angular distribution curves. Fig.3 displays the contribution curves for different intermediate diquark states. In each p_t distribution, a noticeable peak emerges at approximately several GeV, followed by a logarithmic decline in the high p_t region. In all three distinct kinematic distributions, it is consistently evident that the $\bar{3}[{}^3S_1]$ configurations maintain prominence across the entire range, while contributions from other states are small.

Finally, we delve into a brief discussion of the theoretical uncertainties inherent in our calculations, stemming from three main sources: the heavy quark mass m_c , the renormalization scale μ , and the LDMEs. It's worth noting that uncertainties originating from $h_{\bar{3}}$ and $h_{\mathbf{6}}$ have been omitted due to the lack of reported errors in the literature. As mentioned earlier, these coefficients represent global factors, and their influence on production outcomes can be further refined with more precise values. Table 3 demonstrates the impact of changing the value of m_c within the range of 1.8 ± 0.1 GeV while keeping $\mu = \sqrt{M_{\Xi_{cc}}^2 + p_t^2}$ constant. As observed in the table, even small variations in the heavy quark mass can result in substantial fluctuations in cross-section values. For example, in Table 3, the cross section for $(cc)_{\bar{3}}[{}^3S_1]$ varies by approximately 46% with only a 12% change in m_c . This notable sensitivity becomes evident when analyzing the relevant Feynman diagrams, as exemplified in Fig. 1. For photoproduction of Ξ_{cc} considered here, it is noted that the final particles involved in the short-distance processes consist exclusively of c and \bar{c} , while the internal

lines are composed solely of charm and gluon propagators. Therefore, the significant impact of heavy quark masses on the cross section appears to be a reasonable outcome.

Table 4 evaluates the sensitivity to the renormalization scale ($\mu = \mathcal{C}\sqrt{M_{\Xi_{cc}}^2 + p_t^2}$, where $\mathcal{C} = 0.5, 1, 2$), while keeping the value of m_c fixed at 1.8 GeV. Clearly, there is a significant dependence on the renormalization scale, which could suggest the importance of next-to-leading order corrections in α_s . As we confront real-world measurements in the future, high-order calculations become imperative. Taking into account the aforementioned uncertainties, our leading-order calculation results may vary by approximately one order of magnitude. Despite this range of variability, the photoproduction rates of doubly charmed baryons remain significant.

4 Summary

In this work, we have investigated the Ξ_{cc} photoproduction within the framework of non-relativistic QCD specifically focusing on future e^+e^- colliders. Two dominant photoproduction processes are considered, i.e., $\gamma + \gamma \rightarrow \Xi_{cc} + \bar{c} + \bar{c}$ and $\gamma + g \rightarrow \Xi_{cc} + \bar{c} + \bar{c}$. Four P -wave diquark states are included in the calculation and they are $(cc)_{\bar{3}}[{}^1P_1]$, $(cc)_{\mathbf{6}}[{}^3P_0]$, $(cc)_{\mathbf{6}}[{}^3P_1]$ and $(cc)_{\mathbf{6}}[{}^3P_2]$. Upon assuming $h_{\mathbf{6}} = h_{\bar{3}}$, the results demonstrate the photoproduction of P -wave Ξ_{cc} is about one order lower than that of the S -wave. Specifically, at a center-of-mass energy of $\sqrt{S} = 500$ GeV, the cross section for P -wave Ξ_{cc} production is approximately 6% of that for S -wave production. The numerical results further emphasize the crucial role played by the single resolved photoproduction channel $\gamma + g$ in the overall photoproduction process. It gains increasing significance as the collision energy rises. Assuming an integrated luminosity for future e^+e^- collisions on the order of $\mathcal{O}(10^4)$ fb $^{-1}$, approximately 4.8×10^6 S -wave Ξ_{cc} and 2.9×10^5 P -wave Ξ_{cc} baryons would be expected to be produced at a collision energy of $\sqrt{S} = 500$ GeV. The excited doubly charmed baryons are likely to decay into the ground state with nearly 100% probability. Therefore, when faced with precise real-world measurements, their contributions should be thoroughly examined and taken into account.

Acknowledgments

This work was supported in part by the Natural Science Foundation of China under Grants No. 12305083, No. 12147116, No. 12175025, No. 12005028 and No. 12147102, and by the Fundamental Research Funds for the Central Universities under Grant No. 2020CQJQY-Z003.

References

- [1] SELEX collaboration, First Observation of the Doubly Charmed Baryon Ξ_{cc}^+ , [Phys. Rev. Lett.](#) **89** (2002) 112001 [[hep-ex/0208014](#)].
- [2] SELEX collaboration, Confirmation of the double charm baryon $\Xi_{cc}(3520)$ via its decay to $p D + K^-$, [Phys. Lett. B](#) **628** (2005) 18 [[hep-ex/0406033](#)].

- [3] LHCb collaboration,
First Observation of the Doubly Charmed Baryon Decay $\Xi_{cc}^{++} \rightarrow \Xi_c^+ \pi^+$, [Phys. Rev. Lett. **121** \(2018\) 162002 \[1807.01919\]](#).
- [4] LHCb collaboration, Measurement of the Lifetime of the Doubly Charmed Baryon Ξ_{cc}^{++} ,
[Phys. Rev. Lett. **121** \(2018\) 052002 \[1806.02744\]](#).
- [5] J.P. Ma and Z.G. Si,
Factorization approach for inclusive production of doubly heavy baryon, [Phys. Lett. B **568** \(2003\) 135 \[hep-ph/0305079\]](#).
- [6] G.T. Bodwin, E. Braaten and G.P. Lepage,
Rigorous QCD analysis of inclusive annihilation and production of heavy quarkonium, [Phys. Rev. D **51** \(1995\) 1125 \[hep-ph/9407339\]](#).
- [7] S.P. Baranov,
On the production of doubly flavored baryons in p p, e p and gamma gamma collisions, [Phys. Rev. D **54** \(1996\) 3228](#).
- [8] A.V. Berezhnoy, V.V. Kiselev and A.K. Likhoded,
Photonic production of S- and P wave B/c states and doubly heavy baryons, [Z. Phys. A **356** \(1996\) 89](#).
- [9] J. Jiang, X.-G. Wu, Q.-L. Liao, X.-C. Zheng and Z.-Y. Fang,
Doubly Heavy Baryon Production at A High Luminosity e^+e^- Collider, [Phys. Rev. D **86** \(2012\) 054021 \[1208.3051\]](#).
- [10] J. Jiang, X.-G. Wu, S.-M. Wang, J.-W. Zhang and Z.-Y. Fang,
A Further Study on the Doubly Heavy Baryon Production around the Z^0 Peak at A High Luminosity e^+e^- Col
[Phys. Rev. D **87** \(2013\) 054027 \[1302.0601\]](#).
- [11] G. Chen, X.-G. Wu, Z. Sun, Y. Ma and H.-B. Fu,
Photoproduction of doubly heavy baryon at the ILC, [JHEP **12** \(2014\) 018 \[1408.4615\]](#).
- [12] Z.-J. Yang, P.-F. Zhang and Y.-J. Zheng,
Doubly Heavy Baryon Production in e^+e^- Annihilation, [Chin. Phys. Lett. **31** \(2014\) 051301](#).
- [13] Z.-J. Yang and X.-X. Zhao, The Production of Ξ_{bb} at Photon Collider, [Chin. Phys. Lett. **31** \(2014\) 091301 \[1408.5584\]](#).
- [14] X.-C. Zheng, C.-H. Chang and Z. Pan,
Production of doubly heavy-flavored hadrons at e^+e^- colliders, [Phys. Rev. D **93** \(2016\) 034019 \[1510.06808\]](#).
- [15] H.-Y. Bi, R.-Y. Zhang, X.-G. Wu, W.-G. Ma, X.-Z. Li and S. Owusu,
Photoproduction of doubly heavy baryon at the LHeC, [Phys. Rev. D **95** \(2017\) 074020 \[1702.07181\]](#).
- [16] Z. Sun and X.-G. Wu,
The production of the doubly charmed baryon in deeply inelastic ep scattering at the Large Hadron Electron Co
[JHEP **07** \(2020\) 034 \[2004.01012\]](#).
- [17] G. Chen, X.-G. Wu, J.-W. Zhang, H.-Y. Han and H.-B. Fu,
Hadronic production of Ξ_{cc} at a fixed-target experiment at the LHC, [Phys. Rev. D **89** \(2014\) 074020 \[1401.6269\]](#).
- [18] G. Chen, X.-G. Wu and S. Xu,

- Impacts of the intrinsic charm content of the proton on the Ξ_{cc} hadroproduction at a fixed target experiment at [Phys. Rev. D **100** \(2019\) 054022 \[1903.00722\]](#).
- [19] G. Chen, C.-H. Chang and X.-G. Wu, [Hadronic production of the doubly charmed baryon via the proton–nucleus and the nucleus–nucleus collisions at Eur. Phys. J. C **78** \(2018\) 801 \[1808.03174\]](#).
- [20] A.P. Martynenko and A.M. Trunin, [Pair double heavy diquark production in high energy proton–proton collisions, Eur. Phys. J. C **75** \(2015\) 138 \[1405.0969\]](#).
- [21] S. Koshkarev, [Production of the Doubly Heavy Baryons, \$B_c\$ Meson and the All-charm Tetraquark at AFTER@LHC with Dou Acta Phys. Polon. B **48** \(2017\) 163 \[1610.06125\]](#).
- [22] S. Koshkarev and V. Anikeev, [Production of the doubly charmed baryons at the SELEX experiment – The double intrinsic charm approach, Phys. Lett. B **765** \(2017\) 171 \[1605.03070\]](#).
- [23] S. Groote and S. Koshkarev, [Production of doubly charmed baryons nearly at rest, Eur. Phys. J. C **77** \(2017\) 509 \[1704.02850\]](#).
- [24] A.V. Berezhnoy, A.K. Likhoded and A.V. Luchinsky, [Doubly heavy baryons at the LHC, Phys. Rev. D **98** \(2018\) 113004 \[1809.10058\]](#).
- [25] S.J. Brodsky, S. Groote and S. Koshkarev, [Resolving the SELEX–LHCb double-charm baryon conflict: the impact of intrinsic heavy-quark hadroproduction Eur. Phys. J. C **78** \(2018\) 483 \[1709.09903\]](#).
- [26] A.V. Berezhnoy, I.N. Belov and A.K. Likhoded, [Production of doubly charmed baryons with the excited heavy diquark at LHC, Int. J. Mod. Phys. A **34** \(2019\) 1950038 \[1811.07382\]](#).
- [27] X.-G. Wu, [A new search for the doubly charmed baryon \$\Xi_{cc}^+\$ at the LHC, Sci. China Phys. Mech. Astron. **63** \(2020\) 221063 \[1912.01953\]](#).
- [28] Q. Qin, Y.-F. Shen and F.-S. Yu, [Discovery potentials of double-charm tetraquarks, Chin. Phys. C **45** \(2021\) 103106 \[2008.08026\]](#).
- [29] J.-J. Niu, L. Guo, H.-H. Ma, X.-G. Wu and X.-C. Zheng, [Production of semi-inclusive doubly heavy baryons via top-quark decays, Phys. Rev. D **98** \(2018\) 094021 \[1810.03834\]](#).
- [30] J.-J. Niu, L. Guo, H.-H. Ma and X.-G. Wu, [Production of doubly heavy baryons via Higgs boson decays, Eur. Phys. J. C **79** \(2019\) 339 \[1904.02339\]](#).
- [31] P.-H. Zhang, L. Guo, X.-C. Zheng and Q.-W. Ke, [Excited doubly heavy baryon production via \$W^+\$ boson decays, Phys. Rev. D **105** \(2022\) 034016 \[2202.01579\]](#).
- [32] X. Luo, Y.-Z. Jiang, G.-Y. Zhang and Z. Sun, [Doubly-charmed baryon production in \$Z\$ boson decay, 2206.05965](#).
- [33] X. Luo, H.-B. Fu and H.-J. Tian, [Investigation of \$Z\$ -boson decay into and baryons within the NRQCD factorization approach*, Chin. Phys. C **47** \(2023\) 053102 \[2208.07520\]](#).

- [34] H.-H. Ma, J.-J. Niu and X.-C. Zheng, Excited doubly heavy baryons production via top-quark decays, [Phys. Rev. D **107** \(2023\) 014006](#) [[2210.03306](#)].
- [35] C.-H. Chang, J.-X. Wang and X.-G. Wu, GENXICC: A Generator for hadronic production of the double heavy baryons $\Xi(cc)$, $\Xi(bc)$ and $\Xi(bb)$, [Comput. Phys. Commun. **177** \(2007\) 467](#) [[hep-ph/0702054](#)].
- [36] C.-H. Chang, J.-X. Wang and X.-G. Wu, GENXICC2.0: An Upgraded Version of the Generator for Hadronic Production of Double Heavy Baryons $\Xi(cc)$, [Comput. Phys. Commun. **181** \(2010\) 1144](#) [[0910.4462](#)].
- [37] X.-Y. Wang and X.-G. Wu, GENXICC2.1: An Improved Version of GENXICC for Hadronic Production of Doubly Heavy Baryons, [Comput. Phys. Commun. **184** \(2013\) 1070](#) [[1210.3458](#)].
- [38] FCC collaboration, FCC-ee: The Lepton Collider: Future Circular Collider Conceptual Design Report Volume 2, [Eur. Phys. J. ST **228** \(2019\) 261](#).
- [39] C.S. Group, CEPC Conceptual Design Report: Volume 1 - Accelerator, [1809.00285](#).
- [40] CEPC STUDY GROUP collaboration, CEPC Conceptual Design Report: Volume 2 - Physics & Detector, [1811.10545](#).
- [41] ILC collaboration, International Linear Collider Reference Design Report Volume 2: Physics at the ILC, [0709.1893](#).
- [42] J. Erler, S. Heinemeyer, W. Hollik, G. Weiglein and P.M. Zerwas, Physics impact of GigaZ, [Phys. Lett. B **486** \(2000\) 125](#) [[hep-ph/0005024](#)].
- [43] M. Klasen, B.A. Kniehl, L.N. Mihaila and M. Steinhauser, Evidence for color octet mechanism from CERN LEP-2 $\gamma\gamma \rightarrow J/\psi + X$ data, [Phys. Rev. Lett. **89** \(2002\) 032001](#) [[hep-ph/0112259](#)].
- [44] R. Li and K.-T. Chao, Photoproduction of J/ψ in association with a $c\bar{c}$ pair, [Phys. Rev. D **79** \(2009\) 114020](#) [[0904.1643](#)].
- [45] X.-J. Zhan and J.-X. Wang, Prompt J/ψ photoproduction within the non-relativistic QCD framework at the CEPC, [Eur. Phys. J. C **80** \(2020\) 740](#) [[2005.08816](#)].
- [46] X.-J. Zhan and J.-X. Wang, Inclusive $\Upsilon(1S, 2S, 3S)$ photoproduction at the CEPC, [Chin. Phys. C **45** \(2021\) 023112](#).
- [47] X.-J. Zhan, X.-G. Wu and X.-C. Zheng, Inclusive J/ψ photoproduction at the ILC within the framework of non-relativistic QCD, [JHEP **09** \(2022\) 050](#) [[2207.01763](#)].
- [48] X.-J. Zhan, X.-G. Wu and X.-C. Zheng, Photoproduction of the Bc meson at future e+e- colliders, [Phys. Rev. D **106** \(2022\) 094036](#) [[2211.09003](#)].
- [49] I.F. Ginzburg, G.L. Kotkin, V.G. Serbo and V.I. Telnov, Colliding gamma e and gamma gamma Beams Based on the Single Pass Accelerators (of Vlepp Type), [Nucl. Instrum. Meth. **205** \(1983\) 47](#).

- [50] V.I. Telnov, Problems of Obtaining $\gamma\gamma$ and γe Colliding Beams at Linear Colliders, [Nucl. Instrum. Meth. A **294** \(1990\) 72](#).
- [51] M. Gluck, E. Reya and I. Schienbein, Radiatively generated parton distributions of real and virtual photons, [Phys. Rev. **D60** \(1999\) 054019](#) [[hep-ph/9903337](#)].
- [52] A.F. Falk, M.E. Luke, M.J. Savage and M.B. Wise, Heavy quark fragmentation to baryons containing two heavy quarks, [Phys. Rev. D **49** \(1994\) 555](#) [[hep-ph/9305315](#)].
- [53] V.V. Kiselev, A.K. Likhoded and M.V. Shevlyagin, Double charmed baryon production at B factory, [Phys. Lett. B **332** \(1994\) 411](#) [[hep-ph/9408407](#)].
- [54] E. Bagan, H.G. Dosch, P. Gosdzinsky, S. Narison and J.M. Richard, Hadrons with charm and beauty, [Z. Phys. C **64** \(1994\) 57](#) [[hep-ph/9403208](#)].
- [55] A. Berezhnoy, V. Kiselev, A. Likhoded and A. Onishchenko, Doubly charmed baryon production in hadronic experiments, [Phys. Rev. D **57** \(1998\) 4385](#) [[hep-ph/9710339](#)].
- [56] D. Binosi and L. Theussl, JaxoDraw: A Graphical user interface for drawing Feynman diagrams, [Comput. Phys. Commun. **161** \(2004\) 76](#) [[hep-ph/0309015](#)].
- [57] V.V. Kiselev, A.K. Likhoded, O.N. Pakhomova and V.A. Saleev, Mass spectra of doubly heavy Omega QQ' baryons, [Phys. Rev. D **66** \(2002\) 034030](#) [[hep-ph/0206140](#)].